ACS APPLIED MATERIALS & INTERFACES

Research Article

www.acsami.org

Organophophorous Ester Degradation by Chromium(III) Terephthalate Metal–Organic Framework (MIL-101) Chelated to *N,N*-Dimethylaminopyridine and Related Aminopyridines

Sa Wang,[†] Lev Bromberg,[†] Heidi Schreuder-Gibson,[‡] and T. Alan Hatton*,[†]

[†]Department of Chemical Engineering, Massachusetts Institute of Technology, Cambridge, Massachusetts 02139, United States

[‡]U.S. Army Natick Soldier Research, Development & Engineering Center, Natick, Massachusetts 01760, United States

Supporting Information

ABSTRACT: Porous materials based on chromium(III) terephthalate metal organic frameworks (MOF) MIL-101(Cr) and their complexes with dialkylaminopyridines (DAAP) were synthesized via a DAAP-MOF complexation, and tested for hydrolytic degradation of organophosphorous esters such as diethyl 4-nitrophenyl phosphate (paraoxon). Elemental analysis, TGA, XRD, FT-IR, TEM, SEM, and nitrogen adsorption measurements indicated that the DAAP units were incorporated into MIL-101 pores by complexation, keeping the parent framework intact. The DAAP-MOF enabled facile paraoxon hydrolysis in water/acetonitrile mixtures under ambient conditions (100% conversion after 24 h at pH 10). The MOF-DAAP complexes showed synergistic effects, being 7-fold and 47-fold more active than the parent MIL-101 or DAAP materials, respectively. The high hydrolysis reaction turnover was realized by simultaneous action of the Lewis acid Cr(III) center of the MOF as well as the electron-rich nucleophile, DAAP. This study demonstrates a simple and efficient method of generating catalytically active MOF materials for environmental detoxification as well as defensive applications.

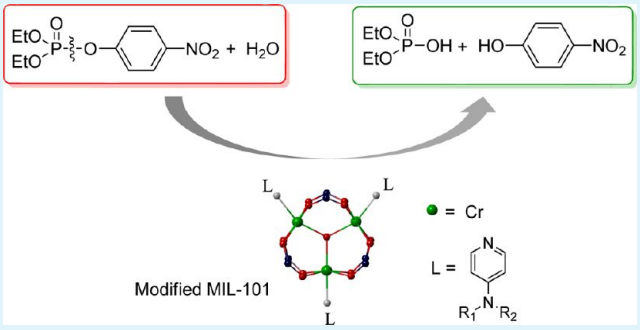

KEYWORDS: *metal–organic framework, aminopyridines, catalysis, organophosphorous ester hydrolysis, paraoxon*

INTRODUCTION

Metal–organic frameworks (MOFs) are porous crystalline solids constructed from metal ions or clusters interconnected by bi- or multipodal organic ligands.[1−5] The high surface area, large porosity, and modular inorganic/organic hybrid structure of the MOF materials prompted exploration of their potential applications in the areas of adsorption, separation, sensing, catalysis, and biomedicine.[6−20] MOFs possess multiple functional sites (metals and/or linkers) that can be rationally designed or tuned; their regular, well-defined pore structures can serve as nanoreactors allowing for uninhibited transport of reactants and products, thus accelerating the reaction rate.[2,18] Approaches for MOF functionalization have concentrated on modification of the framework itself in the process of synthesis (through either the metal site[21,22] or the organic linker[23,24] with a catalytic property), encapsulation of active species,[25,26] or postsynthetic modification.[27,28] Our ongoing research has focused on encapsulation of polyoxometalates such as phosphotungstic acid in MOFs for the purpose of imparting Lewis acid properties to the resulting composites.[29,30] Alternatively, we employed covalent modification of the primary amino groups of the MOF for functionalization with nucleophilic 4-methylaminopyridine (4-MAP).[31] The resulting 4-MAP-modified MOF exhibited facile catalysis of organophorous (OP) esters in aqueous media. Encouraged by these results, in the present work, we address the question whether MOFs modified with organic ligands with nucleophilicity superior to that of 4-MAP would catalyze OP degradation. For modification, we chose a simple complexation between the unsaturated metal sites of the MOF and the nucleophilic ligands, dialkylaminopyridines (DAAP).

Our choice of the parent MOF was MIL-101(Cr), because of its rigid zeotype crystal structure with extremely high surface area ($S_{BET} \approx 4100 \pm 200$ m^2g^{-1}) and relatively large pores (29 and 34 Å with microporous windows of ca. 12 and 16 Å, respectively) that allow accessibility of reactants to active centers.[29,32] Furthermore, MIL-101 is relatively stable in air, water, and most organic solvents at elevated temperatures.[32−34] MIL-101 contains Cr(III) ions that can include coordinatively unsaturated metal sites (CUS), rendering this material a Lewis acid and allowing postsynthetic functionalization via chelating of active species.[35,36] There have been several reports on utilization of the CUS of MIL-101 in the catalysis of cyanosilylation of aldehydes,[37] allylic oxidation of alkenes with TBHP,[38] sulfoxidation of thioethers with H_2O_2,[39] Knoevenagel condensation (CUS modified by diamines),[35]

Received: October 16, 2012
Accepted: January 22, 2013
Published: January 22, 2013

and aldol condensations.[30,36] In this work, we prepared a series of functionalized MOF materials by coordinatively attaching different supernucleophilic dialkylaminopyridine (DAAP) ligands onto the CUS of MIL-101. The resulting complexes showed remarkable reactivities, enabling the hydrolytic degradation of paraoxon at ambient temperature. Notably, we found that the presence of both CUS (Cr(III)) and the electron-rich nucleophile (DAAP) is required for the OP hydrolysis to occur at high yields.

EXPERIMENTAL SECTION

Materials. Terephthalic acid (TPA, 98%), chromium nitrate nonahydrate ($Cr(NO_3)_2{\cdot}9H_2O$, 99%), 4-pyrrolidinopyridine (PyrP, 98%), 4-morpholinopyridine (MorP, 97%), *O*,*O*-diethyl *O*-(4-nitrophenyl) phosphate (paraoxon-ethyl, 98%), 4-morpholinepropanesulfonic acid (MOPS, ≥99.5% titration) 4-(2-hydroxyethyl)piperazine-1-ethanesulfonic acid (HEPES, ≥99.5% titration), 2-(cyclohexylamino)-ethanesulfonic acid (CHES, 99%), and anhydrous toluene (99.8%) were obtained from Sigma-Aldrich Chemical Co. Tetramethylammonium hydroxide (TMAOH, 10% in water), dimethylaminopyridine (DMAP, 99%) and *N*-(3-aminopropyl)-*N*-methylaniline (APMA, ≥96.0% by GC) were obtained from VWR International. All other reagents and solvents were of highest purity available and were used without further purification.

Preparation of MOF Catalysts.

(a) Synthesis of MIL-101. Terephthalic acid (664 mg, 4 mmol) was added to an alkali solution (TMAOH, 20 mL, 0.05 mol/L) and stirred at room temperature for 10 min, following which $Cr(NO_3)_2{\cdot}9H_2O$ (1.6 g, 4 mmol) was added, and the mixture was stirred for another 20 min. The resulting mixture was transferred into a 50 mL Teflon-lined autoclave, and kept in an electric oven at 210 °C for 24 h. After cooling to ambient temperature, the green powder was collected by repeated centrifugation and washing with deionized water. The solid was resuspended in 60 mL of DMF and sonicated for 1 h at 70 °C to remove any terephthalic acid not incorporated into the MOF material. The mixture was centrifuged and washed with water, ethanol and acetone. The product was finally dried under vacuum at room temperature until constant weight.

(b) Functionalization of MIL-101 with DAAP ligands. In a typical procedure, the obtained MIL-101 was first dehydrated or activated at 150 °C under vacuum for 24 h. Then the activated MIL-101 (0.3 g, ~0.44 mmol) was suspended in 25 mL of anhydrous toluene. To the suspension, 1.76 mmol of either DMAP (A, 215 mg), PyrP (B, 261 mg), MorP (C, 289 mg), or APMA (D, 289 μL) was added, and the mixture was stirred under reflux for 12 h under argon atmosphere. The product was recovered by filtration and washed with ethanol and acetone. The final product was dried overnight under vacuum at ambient temperature.

Paraoxon Hydrolysis. A stock solution of 50 mM buffer solution in D_2O (MOPS for pH 7.0, HEPES for pH 8.0, CHES for pH 9.0 and 10.0) and a solution of 50 mM paraoxon in acetonitrile were prepared.[40] An appropriate amount of catalyst was weighed into a small reaction vial. At time t_0, 900 μL of the buffer solution and 100 μL of the paraoxon solution were injected into the vial. The resulting suspension was mixed and stirred at room temperature. At a certain reaction time *t*, the mixture was taken out of the vial and centrifuged in *a microcentrifuge tube at 13 000 g for 15 min*. The upper clear solution was taken immediately for NMR measurement. The kinetics of paraoxon esterolysis with or in the absence of catalyst was followed by ^{31}P NMR. The reaction conversions (*F*) at different time intervals were calculated from the ratios of the peak integration of the product (diethyl phosphate, 0.70 ppm) vs the sum of peak integrations of the product and the starting material (paraoxon, 6.62 ppm) in ^{31}P NMR (eq 1),

$$F = \frac{I_p}{I_p + I_s} \times 100\% \quad (1)$$

where I_s and I_p are the integrations of the signals corresponding to the starting material and the product at given time, respectively. The reaction was found to follow pseudofirst-order reaction kinetics (eq 2), and the observed reaction rate constant k_{obs} was obtained from the initial slope of linear plots of $\ln(1 - F)$ vs *t*. The reaction half-life ($t_{1/2}$) was calculated using this value of k_{obs} in eq 3. In what follows, C_{cat} represents catalyst concentration.

$$\ln(1 - F) = -k_{obs}t \quad (2)$$

$$t_{1/2} = \ln(2)/k_{obs} \quad (3)$$

Characterization Methods. NMR data were recorded at room temperature on a Bruker Avance-400 spectrometer equipped with a Magnex Scientific superconducting magnet and a 5 mm VT X/H (BBO) probe. ^1H and ^{31}P NMR spectra were recorded at 400.01 and 161.98 MHz, respectively, and the chemical shifts (δ) are given in ppm. The reaction milieu consisted of 90% D_2O and 10% acetonitrile. For ^{31}P NMR, 128 scans were collected for each spectrum using 85% phosphoric acid solution in D_2O as an external reference (0 ppm).

TEM and SEM were performed on a JEOL 200-CX transmission electron microscope and a JEOL 6700F field-emission gun scanning electron microscope, respectively, to determine the MOF particle size and morphology. TEM samples were prepared by placing drops of the MOF suspension in ethanol on carbon-coated 200 mesh copper grids and imaged at an accelerating voltage of 120 kV. SEM samples were prepared by placing drops of the MOF suspension in ethanol on silicon wafers followed by solvent evaporation, and the images were collected under an acceleration voltage of 5 kV and working distance of 5−6 mm with a standard secondary electron detector.

Powder X-ray Diffraction (XRD) patterns were acquired with a PANalytical Multipurpose Diffractometer equipped with an X'Celerator high-speed detector coupled with a Ni β-fileter and using the Cu Kα radiation. Samples were packed densely in a 0.5 mm deep well on a zero-background holder. Programmable divergence slits were used to illuminate a constant length of the samples (8 mm), so that the constant volume assumption was preserved. The operating power of the diffractometer was set at 45 kV and 40 mA, and the diffraction data were collected between 1 and 30° (2θ) with a total scan time of 3 h.

BET surface area measurements were conducted using a Micromeritics ASAP2020 apparatus at liquid nitrogen temperature (77 K). Prior to each adsorption measurement, the sample was degassed at 323 K under vacuum for 16 h. The specific surface areas were evaluated using the Brunauer−Emmett−Teller (BET) method in the P/P_0 range of 0.06−0.20. Pore size distribution curves were calculated using the Barrett−Joyner−Halenda (BJH) method from the desorption branch of the isotherms and pore sizes were obtained from the peak positions of the distribution curves. The pore volume was taken by a single point method at $P/P_0 = 0.98$.

FTIR spectra were recorded with KBr pellets containing the samples on a Nicolet Magna 860 Fourier transform infrared spectrometer. Thermogravimetric analyses were carried out at a ramp rate of 5 °C/min under a nitrogen flow with a model Q50 thermogravimetric analyzer (TA Instruments, Inc.). Elemental analyses were performed by a commercial laboratory using high temperature combustion (for C/H/N) and inductively coupled plasma optical emission spectrometry (ICP-OES, for metal Cr) methods.

RESULTS

Catalyst Synthesis and Characterization. In the present work, at variance with the original method by Férey and his group,[32] we avoided using hydrofluoric acid in the hydrothermal synthesis of MIL-101 MOF, and employed an optimized $TMAOH/Cr(NO_3)_3/TPA/H_2O$ (0.25/1/1/280) alkaline medium.[41] MOF MIL-101 can be formed in water at pH ~2.6.[29,41,42] A higher concentration of terephthalate anions (pH > pK_a) at higher pH facilitates the process of Cr^{3+}-terephthlatate complexation and the formation of Cr^{3+}-terephthlatate trimers (nuclei).[29] As reported by Férey et

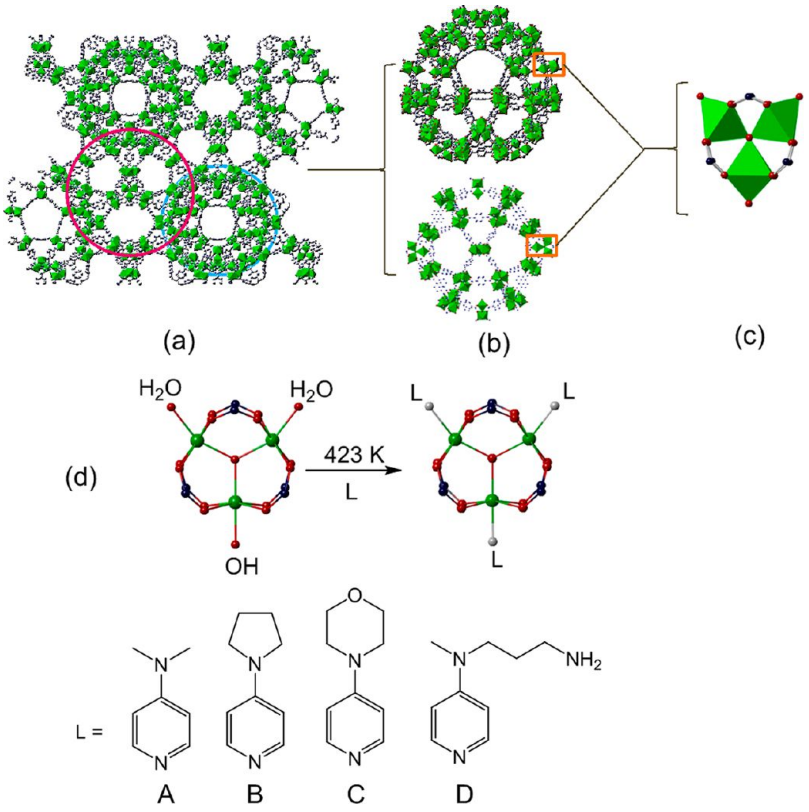

Figure 1. Schematic representation of (a) the unit cell of MIL-101 crystal structure with the boundaries of two types of cages (large cage shown in pink, and small cage is shown as a blue circle); (b) polyhedral model view of the two cages; (c) the trimeric building block sharing an oxygen center and chelated by six carboxylates. Chromium octahedra, oxygen, and carbon atoms are in green, red, and blue, respectively. (d) Evolution of unsaturated metal sites of MIL-101 after vacuum heating, and postmodification of dehydrated MIL-101 through coordination of DAAP-type molecules onto its chromium unsaturated sites. The unit structure depicted corresponds to the published structure of chromium terephthalate MIL-101[32] with formula $Cr_3OH(H_2O)_2O[(O_2C-C_6H_4-(CO_2)]_3$, wherein fluoride is substituted with −OH, as we utilized HF-free synthesis of the MOF.[29] The presense of three ligands (L) per unit is shown, which corresponds to the structures of MIL-101-A, MIL-101-B, and MIL-101-C (Table 1), based on elemental analyses. Crystal structures depicted were built utilizing published lattice parameters[29,32] and applying Crystal Maker software.

Table 1. Compositional Analysis of As-Prepared MOF Catalysts[a]

sample	N (wt %)	Cr (wt %)	L:Cr molar ratio	L loading (mmol/g)	Cr(III) (mmol/g)	content of catalytic units per g of solids (mmol/g)[b]
MIL-101-A	5.54	11.0	0.94	2.0	2.1	0.96
MIL-101-B	5.07	10.4	0.91	1.8	2.0	0.89
MIL-101-C	5.32	10.8	0.91	1.9	2.1	0.85
MIL-101-D	5.81	11.7	0.61	1.4	2.3	0.99

[a]L denotes ligand. [b]Catalytic units include chromium terephthalate unit chelated to the corresponding ligand depicted in Figure 1, with molecular weight computed using elemental analysis results.

al.,[32] MIL-101 can be described by a molecular formula of $[Cr_3(OH)(H_2O)_2O[O_2CC_6H_4CO_2]_3{\cdot}nH_2O$ (where n varies)] and is composed of a 3D network of chromium atoms connected through benzene dicarboxylate groups. Two types of mesoporous cages (~29 and 34 Å) are generated in the MIL-101 crystal structure, and they are accessible through five or six membered ring windows (ca. 12 and 16 Å) (Figure 1a, b). Both of the two cages are built on a μ_3-O bridged trimeric Cr(III) cluster chelated by three carboxylic functions (Figure 1c). Indeed, each Cr(III) center has one remaining coordination site occupied by a water (or OH) molecule. Removal of these terminal OH/H_2O groups from the cluster may introduce numerous CUS in the structure, which can either act as Lewis acids or coordinate with functional ligands (Figure 1d).

We selected four DAAP analogs [4-dimethylaminopyridine (A), 4-pyrrolidinopyridine (B), 4-morpholinopyridine (C), 4-(3-aminopropyl)-methylaniline (D)] to be incorporated into the MIL-101 framework (Figure 1d). Dimethylaminopyridine (DMAP) and its analogs or congeners have been reported to be highly nucleophilic catalysts in many organic reactions such as acylation, transesterification, esterolysis, alkylation, etc.[45−48] The pyridine group has been frequently used in organometallic catalysts as an auxiliary complexing agent.[48−50] By combining the CUS and DAAP ligand together through complexation, we anticipated that the new MIL-101/DAAP hybrids would be active in promoting the OP esters degradation. Postmodification of MIL-101 was achieved by mixing its dehydrated form with a ligand, followed by refluxing in anhydrous toluene for 24 h.[35,36] The pyridine moieties of the DAAP compounds were chelated to the unsaturated metal sites of the MIL-101 framework through the Lewis acid−base complexation. The aqua ligands of MOF can be replaced by other nucleophilic

dx.doi.org/10.1021/am302359b | ACS Appl. Mater. Interfaces 2013, 5, 1269−1278

units such as alcohol or pyridine,[51,52] with pyridine strongly adsorbed onto the CUS formed in MIL-101 with high stabilization energy.[52]

The as-synthesized functional MOF materials (MIL-101-A, MIL-101-B, MIL-101-C, and MIL-101-D) were characterized using a variety of different techniques. Elemental analysis (Table 1) shows that about 0.9 mol aminoalkylpyridine molecules per mol of Cr(III) were incorporated in the first three MOF materials. The loaded amounts exceed those for the previously reported for MIL-101 frameworks that were modified with primary amines or pyridinyl compounds (0.3−0.6 molecule per Cr atom),[35,36] thus demonstrating high efficiency of our synthesis. Ligand D was loaded into the MIL-101 structure with a ligand-to-Cr(III) molar ratio of 0.6:1. This relatively smaller ratio, compared to the other three samples (Table 1) may have resulted from multichelation of this ligand to the unsaturated Cr centers in MIL-101 via both of its two coordination sites: the primary amine and the pyridine groups. Both of the groups could coordinate to the Cr atoms that are located at the two adjacent elementary units in the MOF. The loading contents of ligands A−C in the MIL-101 material are calculated to be around 1.8−2.0 mmol/g, higher than the ligand D (1.4 mmol/g) in MIL-101. The chromium contents in four different MOF catalysts are quite similar (2.0−2.2 mmol/g).

The thermogravimetric analysis (TGA) of MIL-101 and MIL-101-A is shown in Figure 2. Two weight-loss steps were

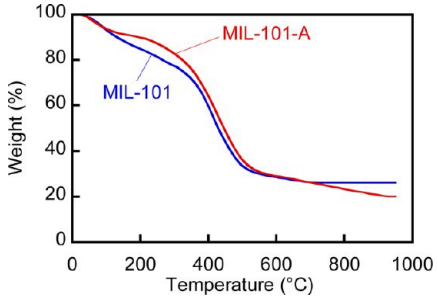

Figure 2. TGA profiles of MIL-101 and MIL-101-A under nitrogen atmosphere at a heating rate of 5 °C/min.

observed in the TGA profiles. The first step, in the range of 25−350 °C, is related to the loss of the guest water and solvent molecules. About 27% and 23% weight losses were observed for MIL-101 and MIL-101-A, respectively. The 4% differences indicate that water in MIL-101-A could have been replaced by the DMAP molecules. The decomposition of the organic moieties and collapse of the framework were observed in the range of 350−570 °C. Both MIL-101 (ca. 44% losses) and MIL-101-A (ca. 49% losses) gave the final ∼29% residual weight after decomposition, corresponding to the residual Cr_2O_3 solids. As their TGA results show, the MIL-101 materials are stable up to 350 °C, which corresponds well with the previously reported stability.[29]

The morphologies of MIL-101 and MIL-101-A were visualized by SEM and TEM (Figure 3). The TEM image of bare MIL-101 shows that it is composed of well-defined small cuboctahedral-shaped crystals, reflecting the cubic symmetry of the MIL-101 crystal (Figure 3a).[29,32] The SEM images of the bare MIL-101 indicate that particles synthesized under our specific conditions possess regular shapes with size ranging from 200 to 400 nm (Figure 3c). Both TEM and SEM images of MIL-101-A reveal similar crystal size and morphology to the bare MIL-101, demonstrating that the structural integrity of MIL-101 was well-preserved after chemical modification by DMAP (Figure 3a, d).

X-ray powder diffraction (XRPD) measurements were employed to identify and probe the crystal structures of modified MIL-101 materials (Figure 4). Both the peak position and relative intensities of the as-prepared MIL-101 are in a good agreement with the simulated pattern from the single crystal data reported by Férey et al.,[32] which confirms the high crystallinity of MIL-101 resulting from our synthesis. No significant diffraction peaks characteristic of TPA species were detected, indicating that a high-purity MIL-101 was obtained.[55] The XRD patterns of functionalized MIL-101 structures show peak patterns almost identical to those of as-synthesized, parent MIL-101. This demonstrates that the framework integrity of MIL-101 was retained after both thermal water removal and chemical modification processes, and is consistent with the high stability of these MOF materials. However, the relative intensities of diffraction peaks from different MIL-101 structures, such as peaks at 8.5 and 9.1° corresponding to (0 6 6) and (1 1 9) planes, respectively,[53] show slight variations for each specific complex. These variations may result from incorporation of DAAP molecules in the MIL-101 crystal structure, and changes in the electronic environment around the Cr atom due to its coordination with pyridine. We did not observe any significant new peaks appearing in the XRD spectra of modified MIL-101 structures, which is consistent with other reports.[35,36]

FTIR spectra were collected on all MIL-101 samples, and FTIR spectra of MIL-101, DMAP, and MIL-101-A are shown in Figure 5. Peaks characteristic of MIL-101 and DMAP were observed in the functionalized MOF, MIL-101-A. The strong bands of MIL-101 at 1625, 1510, and 1410 cm^{-1} were present in MIL-101-A, corresponding to the C═C and O−C═O stretching vibrations of the benzene dicarboxylate organic skeleton.[32] The strong band centered at 3440 cm^{-1} is due to the presence of water molecules in both MIL-101 and MIL-101-A solids. The aliphatic C−H stretching vibrations of DMAP, in the range from 2980 to 2800 cm^{-1}, were also found as weak bands in MIL-101-A. Peaks centered at 1602, 1537, 1518, and 1444 cm^{-1} in DMAP were ascribed to its ring skeleton C═N and C═C vibrations. It is interesting to note that the former three peaks shifted to higher positions to 1650, 1563, and 1549 cm^{-1} in MIL-101-A, which is due to coordination of the pyridine nitrogen in DMAP or other alkylaminopyridines to the Cr(III) Lewis acid center (compare with S-4, S-5, S-6).[52,53] Other characteristic bands of DMAP such as the C−N stretching at 1224 cm^{-1} and C−H bending at 1070 and 808 cm^{-1} also appeared in MIL-101-A.

Nitrogen adsorption−desorption isotherms of the activated MIL-101 and MOF catalysts are shown in Figure 6. BET and Langmuir fits for the activated MIL-101 afforded surface areas of 3490 and 4986 m^2/g, respectively, which are close to reported values.[29,32,47] Using a single point adsorption method, the total pore volume of MIL-101 was estimated to be 1.7 cm^3/g. Compared with bare MIL-101, the functionalized MOF exhibits a decrease in the volume of N_2 adsorbed at $P/P_0 > 0.01$. The BET surface area and total pore volume of MIL-101-A/B/C/D were calculated to be within the range of 1430−1610 m^2/g and 0.7−0.8 cm^3/g, respectively, significantly lower than the corresponding values for activated MIL-101 due to the ligands occupying the cavity space of the MOF. Still, the surface areas of the MOF functionalized by DAAP are larger than those

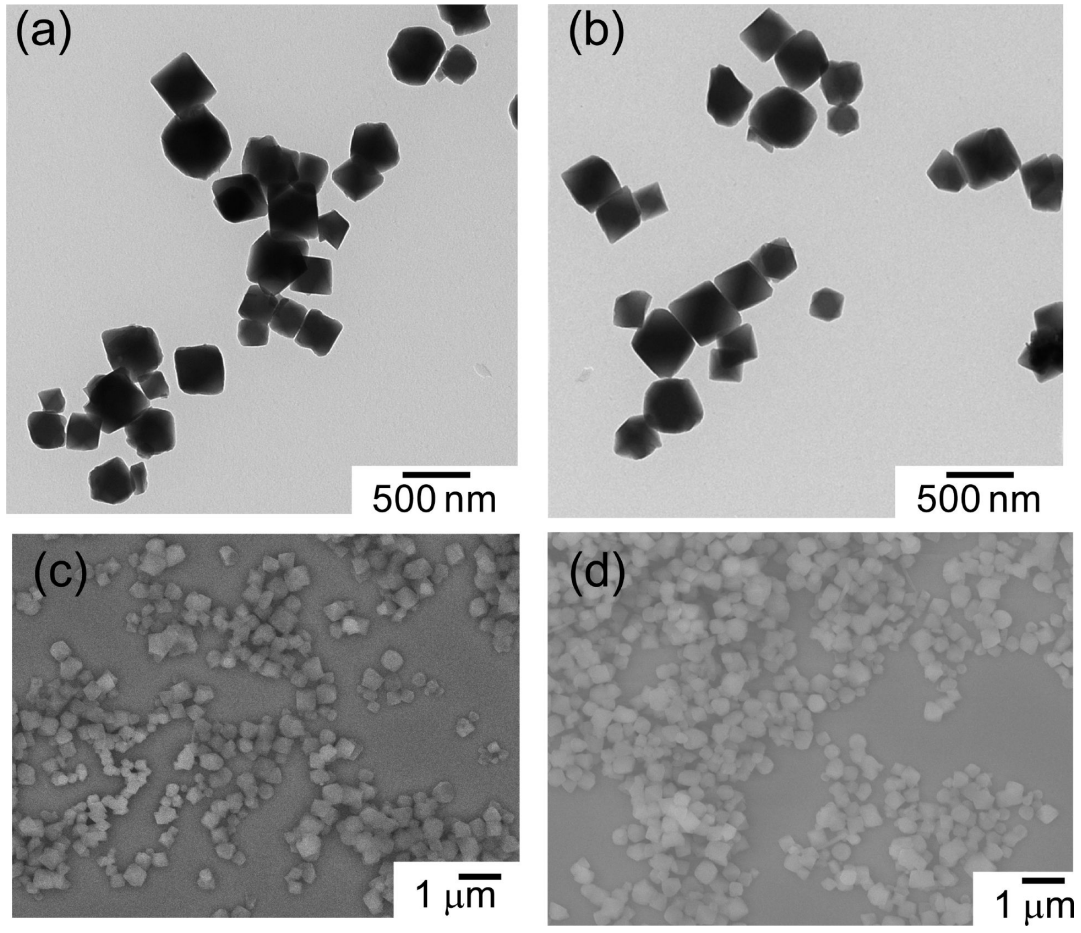

Figure 3. TEM images of (A) MIL-101 and (B) MIL-101-A. SEM images of (C) MIL-101 and (D) MIL-101-A.

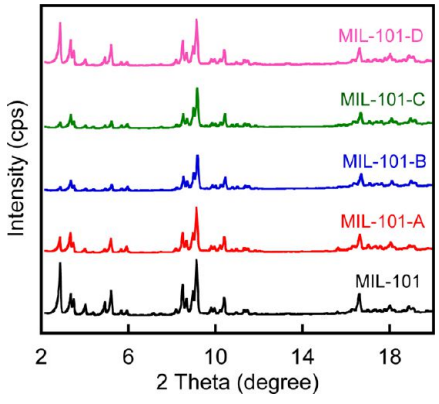

Figure 4. Powder XRD patterns of as-synthesized and postmodified MIL-101: MIL-101, MIL-101-A, MIL-101-B, MIL-101-C, MIL-101-D.

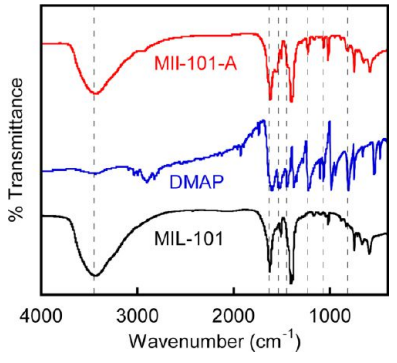

Figure 5. FT-IR spectra of MIL-101, DMAP, and MIL-101-A. Vertical lines show bands at 3440, 1602, 1537, 1518, 1224, 1070, and 808 cm^{-1}.

of most zeolites or silicas (usually <1000 m^2/g).[18] The functionalized MOF materials can be defined as microporous (pore size <2 nm) as their pore sizes are smaller than 1.8 nm after the organic ligand complexation.

Performance of Functionalized MOFs. The performance of MIL-101/DAAP composites was assessed using the hydrolytic degradation of paraoxon, an OP compound that serves as an analog of other organophosphorous pesticides as well as chemical threat agents. The reactions were carried out using 5 mg MIL-101 material per mL solution in a water-acetonitrile (9:1) mixed solvent at ambient temperature. Acetonitrile was used to enable sufficient solubility of paraoxon in the reaction medium. As shown in Scheme 1, the paraoxon decomposition yields diethyl phosphate and *p*-nitrophenol as hydrolytic products. The reaction conversions at different time intervals were monitored by ^{31}P NMR (Figure 7) by measuring the disappearance of the starting material, paraoxon (signal at 6.62 ppm) and appearance of the product, diethyl phosphate (signal at 0.70 ppm, position confirmed with the diethyl phosphate sample). Varying reaction conditions such as pH, catalyst loadings, and the structure of DAAP compounds, were investigated to achieve the optimal settings of the reaction system. We also ran a control set of experiments with unmodified MIL-101 and the DAAP ligands alone.

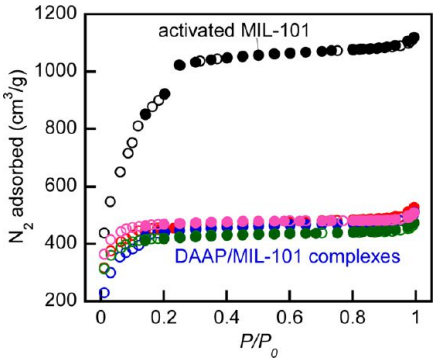

Figure 6. N_2 adsorption−desorption isotherms of activated MIL-101 (black), and MOF catalysts MIL-101-A (red), MIL-101-B (blue), MIL-101-C (green), MIL-101-D (pink) measured at 77 K. Open and filled circles represent adsorption and desorption branches, respectively.

Scheme 1. Catalytic Hydrolysis of Paraoxon with New MOF Composites

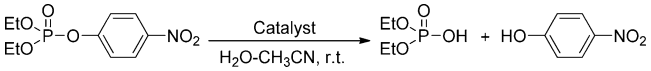

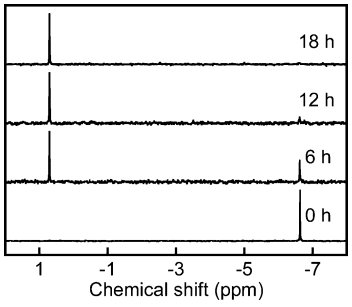

Figure 7. Representative ^{31}P NMR spectra in the study of kinetics of paraoxon hydrolysis. The signals of starting material (paraoxon) and product (diethyl phosphate) appeared at −6.62 and 0.70 ppm, respectively. Reaction conditions: paraoxon 5 mM, catalyst MIL-101-A 5 mg/mL solution, solvent D_2O:CAN (9:1), pH 10.0.

Effect of pH. The effect of pH on the degradation of paraoxon in the presence of MIL-101-A was tested over the pH range from 7 to 10. Control experiments without the addition of any material were also carried out. The spontaneous paraoxon hydrolysis showed almost no conversion under all pHs studied; the reaction at pH 10 gave only 3% conversion after 24 h. In the presence of modified MOF, at pH 7.0 the reaction resulted in 59% conversion after 24 h. Increasing the reaction pH to 8.0 or 9.0 afforded higher conversions of around 86% within the same time period. pH 10.0 resulted in conversion of 92% at 18 h and 100% conversion at 24 h (Table 2). The reaction kinetics results depicted as a plot of reaction conversion vs time are shown in Figure 8(a). The hydrolysis in the presence of MIL-101-A was much faster than the spontaneous reaction. Moreover, the catalyzed reaction rate increased in the following order: pH 7.0 < pH 8.0 ≈ pH 9.0 < pH 10.0. All catalyzed reactions showed good linear fits to pseudofirst-order initial reaction kinetics (Figure 8b), yielding the observed reaction rate constants k_{obs} from the linear slopes of the $\ln(1 - F)$ vs t plots. These parameters, along with the reaction half-life $t_{1/2} = \ln(2)/k_{obs}$, are collected in Table 2. In

Table 2. Parameters of Paraoxon Hydrolysis in the Presence of MIL-101-A under Varying pH

pH	MOF	conversion at 24 h (F)	C_{cat} (mM)	k_{obs} (h^{-1})	$t_{1/2}$ (h)
7.0	none	0	0	n/a	n/a
	MIL-101-A	0.59	4.8	0.037	18.9
8.0	none	0	0	n/a	n/a
	MIL-101-A	0.86	4.8	0.08	8.6
9.0	none	0	0	n/a	n/a
	MIL-101-A	0.86	4.8	0.08	8.5
10.0	none	0.03[a]	0.001	693	n/a
	MIL-101-A	1.0	4.8	0.14	5.0

[a]Calculated from single point linear prediction; that is, $k_{obs} = -[\ln(1-F)]/t$.

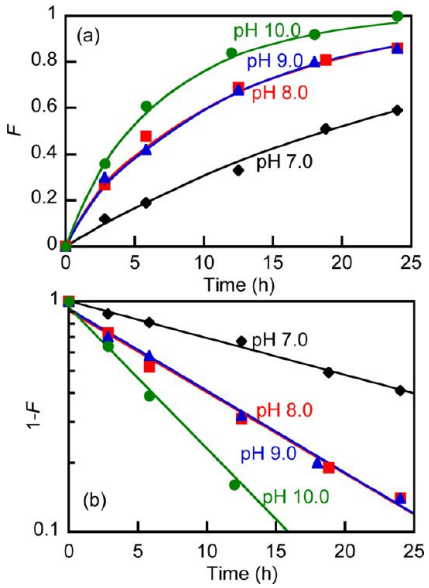

Figure 8. Effects of pH on paraoxon hydrolysis catalyzed by MIL-101-A. (a) Plots of reaction conversion vs time. Reaction conditions: paraoxon 5 mM, MIL-101-A loading, 5 mg/mL solution, solvent D_2O:ACN (9:1), buffer system: pH 7.0 (MOPS), pH 8.0 (HEPES), pH 9.0 (CHES), pH 10.0 (CHES). (b) Pseudo-first-order fits of initial kinetics at different pH (log scale).

the following tests, we used pH 10 to monitor the effects of the material loading and ligand structure on the reaction rates.

Effect of MOF Loading. The effect of the MOF loading on the kinetics of paraoxon hydrolysis was examined at pH 10 with MIL-101-A as the reaction promoter (Figure 9a). It appeared that only the reactions with ≥5 mg MIL-101-A loading went to completion after 24 h. More importantly, the reaction rate seems to increase with higher MIL-101-A loading. The observed reaction rate constant, k_{obs}, can be estimated from the initial slope of the pseudofirst-order reaction kinetics (Table 3). When plotting k_{obs} vs MIL-101/DAAP loading, we found that the reaction rate was linearly proportional to the mass of the MIL-101/DAAP loading x (R^2 = 0.994) (Figure 9b). This phenomenon indicated that the MIL-101/DAAP participated in the reaction rate-determining step (RDS), and the reaction order with respect to the MIL-101/DAAP was determined to be around 1, which is the same as that relative to the substrate paraoxon. Therefore, the reaction rate can be expressed as $r = k_{obs}[\text{paraoxon}] = k'[\text{MIL-101/DAAP}] \times [\text{paraoxon}]$, where the second-order reaction rate constant k'

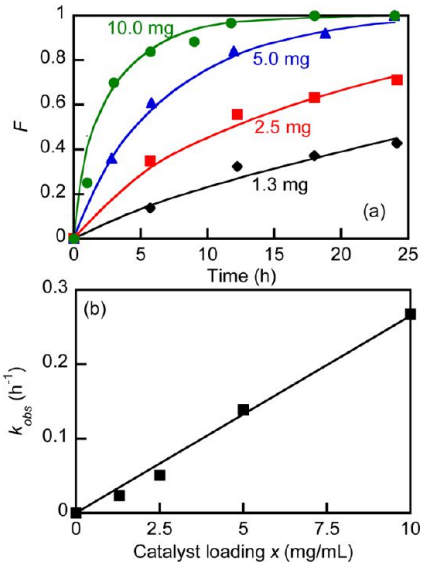

Figure 9. Effects of catalyst loading on the hydrolysis of paraoxon promoted by MIL-101-A. (a) Plots of reaction conversion vs time. Reaction conditions: paraoxon 5 mM, catalyst MIL-101-A x mg/mL solution, solvent D_2O:ACN (9:1), buffer pH 10.0 (CHES). (b) Observed reaction rates (k_{obs}) as a function of the catalyst loading. The solid line is the linear fit of curve of k_{obs} vs x; k' is obtained as the slope of this line.

Table 3. Activities of Paraoxon Hydrolysis Promoted by MIL-101-A under Varying Loadings (pH 10.0)

catalyst loading (mg mL^{-1})	F^a	k_{obs} (h^{-1})	$t_{1/2}$ (h)
1.3	0.43	0.024	29.4
2.5	0.71	0.051	13.7
5.0	1.0	0.14	5.0
10.0	1.0	0.27	2.6

[a]Reaction conversion at 24 h.

was estimated to be 0.027 h^{-1} $(mg/mL)^{-1}$ by linear regression of the k_{obs} vs catalyst loading data in Figure 9b.

Effect of Ligand. With the optimized conditions pH 10.0 and a MIL-101/DAAP loading of 5.0 mg/mL, we investigated the effect of different ligands integrated in MIL-101 on the kinetics of paraoxon degradation. As shown in Figure 1d, compounds B and C were used as analogues of DMAP (compound A) to examine the effect of their different ring structures on the acceleration of paraoxon hydrolysis. We also utilized compound D, which has both a primary amine and a pyridine group, expecting that the combination of two groups may lead to a further reaction rate enhancement. Figure 10 shows the results of a series of tests in which paraoxon hydrolysis was conducted in the presence of four different MIL-101 composites (5 mg per mL of suspension). In these experiments, reactions with MIL-101-A and MIL-101-B appeared to have comparable rates and yielded 100% conversion after 24 h. The reaction in the presence of MIL-101-C showed a slightly lower reaction rate, with 93% conversion after 24 h, whereas the reaction with MIL-101-D produced the slowest reaction rate. The catalyst efficiency follows the order: MIL-101-D < MIL-101-C < MIL-101-A < MIL-101-B. This is in accord with the reported nucleophilicity of the DAAP-type catalysts in reactions such as alcohol acylation or transesterification.[59] The nucleophilic catalysis efficiency by these types of compounds is closely related to the

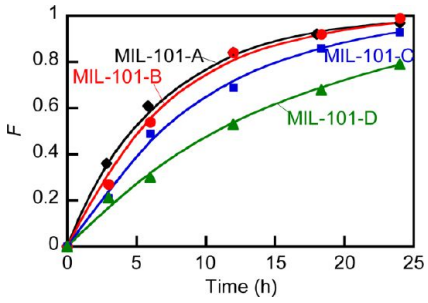

Figure 10. Paraoxon hydrolysis catalyzed by functionalized MOF materials. Reaction conditions: paraoxon, 5 mM; catalyst, 5 mg/mL; solvent, D_2O:ACN (9:1), pH 10.0 (CHES).

stability of their acyl pyridinium intermediates. 4-Pyrrolidinopyridine is generally the most efficient catalyst among 4-amino pyridine derivatives, as its amine N is fixed in a five-member ring and its acyl intermediate is highly stabilized by the electronic communication between the lone pair electrons of the amine and the cation. In our case, DMAP was found to be almost comparable to PyrP in terms of its activity in paraoxon hydrolysis. MorP is a little less effective, as the O in the six-member ring may have on electron-withdrawing effect on the amine N, thus destabilizing the intermediate. APMA is the least efficient, which may result from its relatively larger size in the MOF structure, and thus less freedom to participate in the reaction, or the lower nucleophilic activity of the ligand.

Material Efficiency Analysis. As is seen in Table 5, we observed that: (i) all DAAP-modified MIL-101 composites

Table 4. Activities of Paraoxon Hydrolysis Catalyzed by Different MIL-101 Composites

catalyst	C_{cat} (mM)	F at 24 h	k_{obs} (h^{-1})	$t_{1/2}$ (h)
MIL-101-A	4.8	1.0	0.14	5.0
MIL-101-B	4.5	1.0	0.14	5.0
MIL-101-C	4.3	0.93	0.11	6.2
MIL-101-D	4.9	0.79	0.064	10.8

Table 5. Catalysts Performance in Paraoxon Hydrolysis

reaction	catalyst	C_{cat} (mM)	F^a	$1 \times 10^2 k_{obs}$ (h^{-1})	F^b	$1 \times 10^2 k_{obs}$ (h^{-1})
A	MIL-101-A	4.8[c]	0.86	7.9[e]	1.0	14.2[f]
B	MIL-101-B	4.5[c]	0.81	6.9[e]	1.0	14.2[f]
C	MIL-101-C	4.3[c]	0.66	4.5[e]	0.93	11.2[f]
D	MIL-101-D	4.9[c]	0.57	3.5[e]	0.79	6.4[f]
E	no	0	0	0	0.03	0.10[e]
F	MIL-101	10.4[d]	0.04	0.2[e]	0.12	0.5[e]
G	activated MIL-101	10.4[d]	0.19	0.9[e]	0.40	2.1[e]
H	ligand **A**	9.8[c]	0	0	0.06	0.3[e]
I	activated MIL-101 + ligand **A**	4.7[c]	0.60	3.8[e]	0.92	10.5[e]

[a]Reaction conversion at 24 h under pH 9.0. [b]Reaction conversion at 24 h under pH 10.0. [c]Concentration of the catalytic unit per L of the suspension (Table 1). [d]Concentration of Cr in MIL-101 per L of the suspension. [e]k_{obs} values were calculated from single point linear prediction of first-order reaction kinetics, that is, $k_{obs} = -[\ln(1 - F)]/t$. [f]Values were derived from Table 4.

accelerated reaction with a moderate to high degree of conversion in 24 h at both pH 9 and 10. Among them, MIL-

dx.doi.org/10.1021/am302359b | ACS Appl. Mater. Interfaces 2013, 5, 1269−1278

101-B showed superior activity toward paraoxon hydrolysis. (ii) The spontaneous reactions were extremely slow at both pH 9 and 10 at ambient temperature (0 and 3% conversion, respectively, reaction E). Even at pH 10 the spontaneous reaction rate is about 140- fold slower than the rate of reaction catalyzed by MIL-101-B. (iii) The as-synthesized MIL-101 showed a low catalytic activity toward paraoxon hydrolysis, with only 4 and 12% conversion at pH 9 and 10, respectively, within 24 h (reaction F). (iv) The "activated" MIL-101 (vacuum dehydration of as-synthesized MIL-101 at 150 °C for 24 h) catalyzes the reaction to a significant degree (19 and 40% conversion, reaction G). The activated MIL-101 is 4-fold more effective than as-synthesized MIL-101 because of the higher content of unsaturated Lewis acidic Cr(III) centers after vacuum heating treatment. (v) The ligand DMAP itself did not accelerate the reaction to any significant degree (0 and 6% conversion, reaction H), which is counterintuitive considering that DMAP is a supernucleophilic catalyst in acylation reactions. The activated MIL-101 and DMAP complex showed synergistic acceleration of the reaction (60 and 92% conversion, reaction I). The reaction rate with MIL-101-A is about 7-fold and 47-fold higher than those with its components MIL-101 and DMAP, respectively, and 140-fold faster than the spontaneous hydrolysis at pH 10. The synergistic effect of the MIL-101 and DAAP complexation on the catalytic activity of the studied materials was corroborated by filtration experiments. Namely, the MIL-101-A or MIL-101-B powder was separated from the reaction medium by using a syringe-fitted membrane filter[29] 1 h after the start of the reaction. The separated supernatant was tested for its ability to catalyze the paraoxon hydrolysis. Less than 10% paraoxon conversion was observed in the supernatant after 24 h. That is, because DMAP and its analogues alone that could have been washed off the DAAP-MIL-101 complex were unable to accelerate the paraoxon hydrolysis to a significant degree, filtering our catalysts from the reaction medium effectively stopped the hydrolysis reaction.

DISCUSSION

The discovered acceleration of the paraoxon hydrolysis in the presence of the MIL-101/DAAP materials is catalytic, with the first-order dependence of the observed reaction rate on the initial MIL-101/DAAP loading (i.e., effective catalyst concentration, Figure.9). Such dependence indicates that the catalytic species is the MIL-101/DAAP complex, rather than dissociated species. Such a conclusion is further supported by the absence of the reaction acceleration by the DMAP alone and by the uncovered synergism of the activated MOF complexed with alkylaminopyridine versus weak catalytic activity of the activated MIL-101 alone (Table 5). The catalysts described in the present work are not dissimilar to a variety of organometallic complexes bearing one or more labile ligands.[57] For example, bipyridine complexes of Cu(II) are potent catalysts for the hydrolysis of phosphate esters, in which the metal ion acting as Lewis acid polarizes the P═O double bond, thus facilitating the following nucleophilic attack by the OH^- nucleophile.[58] Because of the presence of accessible metal centers in their 3D crystals, MOFs can behave in a similar fashion, either through the chromium unsaturated sites, or Cr^{3+} ions coordinated to the organic linkers. MOFs are catalytically active in chemical reactions such as cyanosilylation of aldehydes, epoxidation of olefins, etc.[18] Our experimental results demonstrated the effect of Lewis acidity of Cr(III) in MIL-101 on the hydrolysis of the OP esters.

The synergistic rate enhancement by both activated MIL-101 and DAAP complexed to the MOF is analogous to the dual Lewis acid−Lewis base activation in the case of the reaction of cyanation of aldehydes in the presence of chiral Ti(IV) complexes, activated by DMAP as a cofactor.[59,60] The hypothetical catalytic mechanism can be depicted as in Figure.11. The catalysis is initiated by the coordination of the

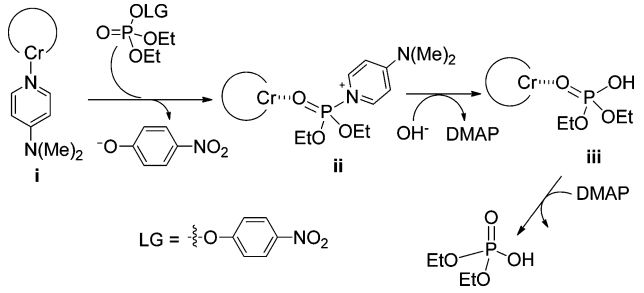

Figure 11. Hypothetical mechanism of the catalytic hydrolysis of paraoxon by MIL-101/DAAP complexes.

Lewis acidic Cr(III) center in MIL-101-DMAP complex (i) to the oxygen of P═O bond in paraoxon to form a new complex. This binding leads to polarization and activation of the P═O bond and facilitates the nucleophilic attack on the phosphorus atom by certain nucleophiles. Some DMAP ligands might dissociate from the Cr(III) center and attack the P of the P-oxo unit bound to and electrophically activated by another Cr(III) center. DMAP, which serves as a Lewis base in the complex, is also an excellent nucleophilic catalyst and can facilitate intramolecular nucleophilic attack on the P═O double bond. The leaving *p*-nitrophenoxy group supplies an additional good electrophile to the reaction zone. The resulting structure ii is more reactive than the starting material, paraoxon, because of the positive charge proximal to the P═O group. Next, nucleophilic addition−elimination between ^-OH and structure ii generates the Lewis acid-coordinated diethyl phosphoric acid (iii), which dissociates to the final product, diethyl phosphate, observed by ^{31}P NMR.

Simultaneous Lewis acid activation of an electrophile and Lewis base activation of a nucleophile analogous to the one depicted in Figure.11 has been introduced and developed in a number of organic syntheses, especially in stereochemical configuration delivery.[61] In our case, the active species in the reactions is the Lewis acid/Lewis base complex Cr(III)/DMAP, where two separate catalysts are coordinatively combined in one catalytic system, and the synergistic activation by two reactive centers allows for significantly higher reaction rate. The Cr(III)/DMAP complex system has also been reported to be an efficient catalyst in the coupling of CO_2 with epoxides or aziridines, where a (Salen)Cr(III)/DMAP complex was used as a homogeneous catalyst.[62−64]

The efficiency of our MOF-based MIL-101/DAAP catalysts in paraoxon hydrolysis compares favorably with established heterogeneous catalytic systems. The observed rate constant with MIL-101-B is about 10-fold larger than that with polymer[65] or nanoparticle[66] matrices with embedded or attached metal-ion complex active centers.

CONCLUSIONS

We discovered that the MIL-101 MOF modified with DAAP ligands is capable of efficient degradation of the organophosphorous ester paraoxon, a biocide widely used for crop protection and a structural analog of chemical warfare agents. The syntheses of MIL-101/DAAP catalysts are straightforward and only require two steps, including activation of MIL-101 and postfunctionalization of the active metal centers in the MOF with DAAP ligands. The complexation of MIL-101 and DAAP resulted in performance superior to that of the MOF or the ligand acting alone, and the synergistic action of the two species in the reaction suggests a double Lewis acid-Lewis base activation mechanism. This work introduces a promising approach toward creation of multifunctional MOF catalysts for various chemical transformations. Future work along these lines will provide MOF-based materials for other industrially important reactive sorption or catalysis processes. We are also studying stability of the catalysts in applications when their exposure to bulk water is not feasible.

ASSOCIATED CONTENT

Supporting Information

Additional characterization of MIL-101-DAAP composites including TGA, TEM, SEM, and FTIR is provided. This material is available free of charge via the Internet at http://pubs.acs.org.

AUTHOR INFORMATION

Corresponding Author

*E-mail: tahatton@mit.edu.

Notes

The authors declare no competing financial interest.

ACKNOWLEDGMENTS

The authors acknowledge the financial support from the Defense Threat Reduction Agency grant HDTR1-09-1-0012. The authors are grateful to Dr. Scott. A. Speakman for help with XRD results interpretation.

REFERENCES

(1) Kitagawa, S.; Kitaura, R.; Noro, S. *Angew. Chem., Int. Ed.* **2004**, *43*, 2334−2375.
(2) Eddaoudi, M.; Moler, D. B.; Li, H.; Chen, B.; Reineke, T. M.; O'Keeffe, M.; Yaghi, O. M. *Acc. Chem. Res.* **2001**, *34*, 319−330.
(3) Tranchemontagne, D. J.; Mendoza-Cortés, J. L.; O'Keeffe, M.; Yaghi, O. M. *Chem. Soc. Rev.* **2009**, *38*, 1257−1283.
(4) Farha, O. K.; Hupp, J. T. *Acc. Chem. Res.* **2010**, *43*, 1166−1175.
(5) O'Keeffe, M.; Yaghi, O. M. *Chem. Rev.* **2012**, *112*, 675−702.
(6) Li, J. R.; Kuppler, R. J.; Zhou, H. C. *Chem. Soc. Rev.* **2009**, *38*, 1477−1504.
(7) Suh, M. P.; Park, H. J.; Prasad, T. K.; Lim, D. W. *Chem. Rev.* **2012**, *112*, 782−835.
(8) Sumida, K.; Rogow, D. L.; Mason, J. A.; McDonald, T. M.; Bloch, E. D.; Herm, Z. R.; Bae, T. H.; Long, J. R. *Chem. Rev.* **2012**, *112*, 724−781.
(9) Li, J. R.; Sculley, J.; Zhou, H, C. *Chem. Rev.* **2012**, *112*, 869−932.
(10) Kreno, L. E.; Leong, K.; Farha, O. K.; Allendorf, M.; Van Duyne, R. P.; Hupp, J. T. *Chem. Rev.* **2012**, *112*, 1105−1125.
(11) Horcajada, P.; Gref, R.; Baati, T.; Allan, P. K.; Maurin, G.; Couvreur, P.; Férey, G.; Morris, R. E.; Serre, C. *Chem. Rev.* **2012**, *112*, 1232−1268.
(12) Meek, S. T.; Greathouse, J. A.; Allendorf, M. D. *Adv. Mater.* **2011**, *23*, 249−267.
(13) Xuan, W.; Zhu, C.; Liu, Y.; Cui, Y. *Chem. Soc. Rev.* **2012**, *41*, 1677−1695.
(14) Cybulski, A.; Moulijn, J. A.; Stankiewicz, A. *Novel Concepts in Catalysis and Chemical Reactors: Improving the Efficiency for the Future*; Wiley−VCH: Weinheim, Germany, 2010; Chapter 4.
(15) Czaja, A. U.; Trukhanb, N.; Müllerb, U. *Chem. Soc. Rev.* **2009**, *38*, 1284−1293.
(16) Farrusseng, D.; Aguado, S.; Pinel, C. *Angew. Chem., Int. Ed.* **2009**, *48*, 7502−7513.
(17) Lee, J. Y.; Farha, O. K.; Roberts, J.; Scheidt, K. A.; Nguyen, S. T.; Hupp, J. T. *Chem. Soc. Rev.* **2009**, *38*, 1450−1459.
(18) Ranocchiari, M.; van Bokhoven, J. A. *Phys. Chem. Chem. Phys.* **2011**, *13*, 6388−6396.
(19) Ma, L.; Abney, C.; Lin, W. *Chem. Soc. Rev.* **2009**, *38*, 1248−1256.
(20) Corma, A.; García, H.; Llabrés i Xamena, F. X. *Chem. Rev.* **2010**, *110*, 4606−4655.
(21) Fujita, M.; Kwon, Y.; Washizu, S.; Ogura, K. *J. Am. Chem. Soc.* **1994**, *116*, 1151−1152.
(22) Schlichte, K.; Kratzke, T.; Kaskel, S. *Microporous Mesoporous Mater.* **2004**, *73*, 81−88.
(23) Shultz, A. M.; Farha, O. K.; Hupp, J. T.; Nguyen, S. T. *J. Am. Chem. Soc.* **2009**, *131*, 4204−4205.
(24) Gascon, J.; Aktay, J.; Hernandez-Alonso, M. D.; van Klink, G. P. M.; Kapteijn, F. *J. Catal.* **2009**, *261*, 75−87.
(25) Sun, C. Y.; Liu, S. X.; Liang, D. D.; Shao, K. Z.; Ren, Y. H.; Su, Z. M. *J. Am. Chem. Soc.* **2009**, *131*, 1883−1888.
(26) Song, J. S.; Luo, Z.; Britt, D. K.; Furukawa, H.; Yaghi, O. M.; Hardcastle, K. I.; Hill, C. L. *J. Am. Chem. Soc.* **2011**, *133*, 16839−16846.
(27) Wang, Z.; Cohen, S. M. *Chem. Soc. Rev.* **2009**, *38*, 1315−1329.
(28) Tanabe, K. K.; Cohen, S. M. *Chem. Soc. Rev.* **2011**, *40*, 498−519.
(29) Bromberg, L.; Diao, Y.; Wu, H.; Speakman, S. A.; Hatton, T. A. *Chem. Mater.* **2012**, *24*, 1664−1675.
(30) Bromberg, L.; Hatton, T. A. *ACS Appl. Mater. Interfaces* **2011**, *3*, 4756−4764.
(31) Bromberg, L.; Klichko, Y.; Chang, E.; Speakman, S.; Straut, C.; Wilusz, E.; Hatton, T. A. *ACS Appl. Mater. Interfaces* **2012**, *4*, 4595−4602.
(32) Férey, G.; Mellot-Draznieks, C.; Serre, C.; Millange, F.; Dutour, J.; Surblé, S.; Margiolaki, I. *Science* **2005**, *309*, 2040−2042.
(33) Jhung, S. H.; Lee, J. H.; Yoon, J. W.; Serre, C.; Férey, G.; Chang, J. S. *Adv. Mater.* **2007**, *19*, 121−124.
(34) Hong, D. Y.; Hwang, Y. K.; Serre, C.; Férey, G.; Chang, J. S. *Adv. Funct. Mater.* **2009**, *19*, 1537−1552.
(35) Hwang, Y. K.; Hong, D. Y.; Chang, J. S.; Jhung, S. H.; Seo, Y. K.; Kim, J.; Vimont, A.; Daturi, M.; Serre, C.; Férey, G. *Angew. Chem., Int. Ed.* **2008**, *47*, 4144−4148.
(36) Banerjee, M.; Das, S.; Yoon, M.; Choi, H. J.; Hyun, M. H.; Park, S. M.; Seo, G.; Kim, K. *J. Am. Chem. Soc.* **2009**, *131*, 7524−7525.
(37) Henschel, A.; Gedrich, K.; Kraehnert, R.; Kaskel, S. *Chem. Commun.* **2008**, 4192−4194.
(38) Maksimchuk, N. V.; Kovalenko, K. A.; Fedin, V. P.; Kholdeevaa, O. A. *Adv. Synth. Catal.* **2010**, *352*, 2943−2948.
(39) Hwang, Y. K.; Hong, D. Y.; Chang, J. S.; Seo, H.; Yoon, M.; Kim, J.; Jhung, S. H.; Serre, C.; Férey, G. *Appl. Catal. A* **2009**, *358*, 249−253.
(40) The buffer allows for the maintenance of constant reaction rate at a particular pH while the formation of acid products will not interfere with the reaction milieu. Acetonitrile was used to improve the miscibility of paraoxon (aqueous solubility at 20 °C, up to 3.6 mg/mL) and aqueous buffer as well as to act as a convenient reactant diluent that did not trigger the reaction prior to contact with the aqueous phase.
(41) Yang, J.; Zhao, Q.; Li, J.; Dong, J. *Microporous Mesoporous Mater.* **2010**, *130*, 174−179.
(42) Khan, N. A.; Jun, J. W.; Jhung, S. H. *Eur. J. Inorg. Chem.* **2010**, 1043−1048.

(43) Khan, N. A.; Kang, I. J.; Seok, H. Y.; Jhung, S. H. *Chem. Eng. J.* **2011**, *166*, 1152−1157.
(44) Spivey, A. C.; Arseniyadis, S. *Angew. Chem., Int. Ed.* **2004**, *43*, 5436−5441.
(45) Vaidyat, R. A.; Mathias, L. J. *J. Am. Chem. Soc.* **1986**, *108*, 5514−5520.
(46) Chen, H. T.; Huh, S.; Wiench, J. W.; Pruski, M.; Lin, V. S. Y. *J. Am. Chem. Soc.* **2005**, *127*, 13305−13311.
(47) Dalaigh, C. Ó.; Corr, S. A.; Gun'ko, Y.; Connon, S. J. *Angew. Chem., Int. Ed.* **2007**, *46*, 4329−4332.
(48) Morrow, J. R.; Trogler, W. C. *Inorg. Chem.* **1988**, *27*, 3387−3394.
(49) Feng, G.; Mareque-Rivas, J. C.; Martín de Rosales, R. T.; Williams, N. H. *J. Am. Chem. Soc.* **2005**, *127*, 13470−13471.
(50) Li, H.; Davis, C. E.; Groy, T. L.; Kelley, D. G.; Yaghi, O. M. *J. Am. Chem. Soc.* **1998**, *120*, 2186−2187.
(51) Chui, S. S. Y.; Lo, S. M. F.; Charmant, J. P. H.; Orpen, A. G.; Williams, I. D. *Science* **1999**, *283*, 1148−1150.
(52) Kim, M. J.; Park, S. M.; Song, S. J.; Wonc, J.; Lee, J. Y.; Yoon, M.; Kim, K.; Seo, G. *J. Colloid Interface Sci.* **2011**, *361*, 612−617.
(53) The peak intensities at low angle (below 4° 2θ) are prone to experimental error, for instance, they can be significantly influenced by surface roughness of the powder sample during preparation. For peaks above 4° 2θ, their intensities are less affected by such an experimental issue.
(54) El-Shall, M. S.; Abdelsayed, V.; Khder, A. S.; Hassan, H. M. A.; El-Kaderi, H. M.; Reich, T. E. *J. Mater. Chem.* **2009**, *19*, 7625−7631.
(55) Masuda, H.; Higashitani, K.; Yoshida, H. *Powder Technology: Fundamentals of Particles, Powder Beds, and Particle Generation*; CRC Press: Boca Raton, FL, 2007; p 86.
(56) Because of instrumental limitations, pore sizes smaller than 1.8 nm cannot be determined.
(57) Behr, A.; Neubert, D. C. P. *Applied Homogeneous Catalysis*; WILEY-VCH Verlag GmbH & Co. KGaA: Weinheim, Germany, 2012.
(58) Wagner-Jauregg, T.; Hackley, B. E., Jr.; Lies, T. A.; Owens, O. O.; Proper, R. *J. Am. Chem. Soc.* **1955**, *77*, 922−929.
(59) Lundgren, S.; Wingstrand, E.; Penhoat, M.; Moberg, C. *J. Am. Chem. Soc.* **2005**, *127*, 11592−11593.
(60) Wingstrand, E.; Lundgren, S.; Penhoat, M.; Moberg, C. *Pure Appl. Chem.* **2006**, *78*, 409−414.
(61) Cahard, D.; Ma, J. A. *Angew. Chem., Int. Ed.* **2004**, *43*, 4566−4583.
(62) Eberhardt, R.; Allmendinger, M.; Rieger, B. *Macromol. Rapid Commun.* **2003**, *24*, 194−196.
(63) Miller, A. W.; Nguyen, S. T. *Org. Lett.* **2004**, *6*, 2301−2304.
(64) Coates, G. W.; Moore, D. R. *Angew. Chem., Int. Ed.* **2004**, *43*, 6618−6639.
(65) Yamazaki, T.; Yilmaz, E.; Mosbach, K.; Sode, K. *Ana. Chim. Acta* **2001**, *435*, 209−214.
(66) Bromberg, L.; Chen, L.; Chang, E. P.; Wang, S.; Hatton, T. A. *Chem. Mater.* **2010**, *22*, 5383−5391.